Electron-positron pair production in Coulomb collisions by 6.4-TeV sulfur ions

C. R. Vane, S. Datz, P. F. Dittner, and H. F. Krause
Physics Division, Oak Ridge National Laboratory, Oak Ridge, Tennessee 38731

R. Schuch and H. Gao
Atomic Physics, Stockholm University, Frescativagen 24, S-104 05 Stockholm 50, Sweden

R. Hutton
Atomic Spectroscopy, University of Lund, Department of Physics, Sölvegatan 14, S-223 62 Lund, Sweden
(Received 4 April 1994)

Angular and momentum distributions have been measured for electron-positron pairs created in peripheral collisions of 6.4-TeV bare sulfur ions with thin targets of Al, Pd, and Au. Singly and doubly differential cross sections are presented for 1–17 MeV/c electrons and positrons detected independently and in coincidence as pairs. Integrated yields for pair production are found to vary as the square of the target nuclear charge. Relative angular and momentum differential cross sections are effectively target independent. Various physical parameters are deduced from the coincident electron and positron data, including probability distributions for the pair transverse momentum, the pair total energy, and the positron fraction of the pair energy. Where possible, results of these measurements are compared with theory.

PACS number(s): 34.90.+q, 12.20.Fv, 34.50.Bw

I. INTRODUCTION

The study of direct electron-positron pair production in Coulomb collisions of high-energy charged particles has a long history, dating from early calculations of Bhabha [1], Racah [2], and Landau and Lifshitz [3] in the 1930's and continuing with modern quantum electrodynamic (QED) calculations through the 1970's [4–8]. Extensive measurements of electron pairs produced by beams of singly charged electron, pion, and proton projectiles, mainly in nuclear track emulsions, have also been performed [9–17] with statistics limited results for pair yields which vary significantly among the measurements. At ultrarelativistic energies, peripheral collisions between heavy, highly charged atoms produce extremely intense, rapidly varying electromagnetic fields which give rise to copious lepton-pair formation. Semiclassical approximations known as equivalent photon or Weizsäcker-Williams methods are often applied, based on Fourier decomposition of the time-dependent Coulomb fields to derive equivalent photon fields [18–20]. These collisions are fundamentally different from those involving singly charged projectiles because the strength of the coupling constant $Z\alpha$, where Z is the charge and α is the fine-structure constant, can be large (≥ 0.5). Lepton-pair production in these systems is especially interesting because the collision strength can be varied continuously, from regions of low charge and energy, where past applications of low-order perturbative theories are suitable, to higher energy and charge regimes where first-order perturbative calculations are known to occasionally give unphysical results [21,22].

Recent progress toward realization of very energetic ion-ion colliders such as the relativistic heavy-ion collider (RHIC) at Brookhaven National Laboratory and the large hadron collider (LHC) at the European Organization for Nuclear Research (CERN) has sparked renewed interest in electromagnetic phenomena at very high energies. A number of theoretical treatments have recently appeared concentrating on lepton-pair production in ultrarelativistic heavy-ion collisions [21–30]. Results of these varied calculations differ substantially in quantitative detail, but generally agree that electron-pair production cross sections should be large, should steadily increase with collision energy, and should lead to single- and possibly multiple-pair formation at rates sufficient to overwhelm contributions from all other processes. In particular, direct Coulomb pair production may obviate the suggested [23] use of lepton signals as a penetrating probe for studying formation and decay of the quark-gluon plasma in ultrarelativistic heavy-ion nuclear collisions [32–34].

In a recent letter [35] we have reported preliminary results of magnetic analysis measurements of positrons emitted in peripheral collisions of 6.4-TeV sulfur ions with thin fixed targets. The only other measurements available for heavy ions accelerated to ultrarelativistic energies are from limited statistics data for relatively high energy pairs measured in emulsion exposures using 0.96- and 3.2-TeV oxygen and 6.4-TeV sulfur ions [36]. Belkacem *et al.* [37,38] have reported pioneering measurements at ~1-GeV/nucleon energies for atomic capture of pair-produced electrons and for total cross sections for low-energy (0.1–2.5 MeV) pair production by uranium and lanthanum ions. Remarkably, nearly half of all pair electrons produced were observed to occupy bound atomic final states for ~230-GeV uranium projectile ions in collisions with a gold target. In this paper we present

measurements and comparisons with theory of angular and momentum distributions and correlations of 1–17-MeV/c electrons and positrons from electron pairs generated by 6.4-TeV sulfur ions in Coulomb collisions with targets of Al, Pd, and Au.

II. EXPERIMENTAL METHODS

Fully stripped 6.4-TeV (200 GeV/nucleon) sulfur ions from the CERN Super Proton Synchrotron (SPS) accelerator were passed through thin foil targets in a high-vacuum chamber centered in the 14-cm gap of a 1-m-long, CERN standard dipole bending magnet located upstream of a large nuclear physics collaboration experiment, WA93 [39]. Measurements of electrons and positrons generated in the targets were performed parasitically with WA93. A schematic of the apparatus is given in Fig. 1, with the magnetic field directed perpendicular to the drawing. Targets were remotely positioned at the center of the vacuum chamber which was isolated from the beamline vacuum (~20 mTorr) by two thin (80 μg/cm^2) plastic film windows. Pressure from the chamber was maintained at less than 5×10^{-5} Torr by two turbomolecular pumps. To minimize backgrounds from electrons scatering from the apparatus, as well as from secondary electron emission from scattering of high-energy collision fragments and conversion of γ rays and high-energy bremsstrahlung, all components of the spectrometer were composed of light materials (aluminum and plastic). The sulfur-ion-beam diameter at the target position was ≤ 6 mm, as determined by beam profile measurements taken 3 m downstream. Electrons and positrons generated by ions in the targets were separated in the nearly uniform ($\pm 3\%$) vertical magnetic field and transported 180° along circular arcs to one of two identical arrays of discrete detectors mounted on either side of the ion beam in the plane containing the chosen target. A schematic of the pair spectrometer, including views from the top and along the beam axis (z), is shown in Fig. 2. Projections of typical calculated trajectories are also shown there for 5-MeV/c electrons and positrons emitted at 0° and 20° with respect to the beam axis.

Each detector array was composed of 41 separate circular (2 cm diam) silicon surface barrier detectors with depletion depths of 300 μm. Thin active depths minimized sensitivity to detection of γ rays and permitted positrons to pass through without annihilation, delivering an average signal amplitude of ~105 keV. Sensitivity to electrons and noise characteristics of each detector were studied prior to electron pair measurements using normally incident 1-MeV β particles from a collimated ^{207}Bi source. Detectors were arranged in five horizontal rows covering 52% of the available area, as shown in Fig. 2(a). The arrangement extended horizontally from 3 to 25 cm from the target center and, vertically, 5.3 cm above and below the ion-beam axis.

For forward emitted electrons or positrons, horizontal (x) displacement of the intercept point of a particle's trajectory with the detector plane is closely proportional to its momentum and is only weakly dependent on launch angle, due to first-order focusing in the plane of dispersion. Particle motion in the vertical (y) direction is unaffected by the magnetic field. Hence, the displacement of the detection position in the horizontal plane from the beam axis corresponds to positron or electron momentum, while vertical (y) displacement corresponds to the vertical component of the transverse momentum (or the vertical component of the polar launch angle for a given total momentum). The apparatus thus constitutes a 180°, homogeneous-field pair spectrometer.

For large polar angles, the dispersive plane focusing effect is weak. However, all electrons and positrons ejected with polar angles $\leq 20°$ would be focused to within the momentum resolution set by the 1.3-cm staggered horizontal spacing of the arrayed detectors. This fixed spacing gave a momentum resolution ($\Delta p/p$) varying from 33% at low momentum to 5.4% at high momentum for a

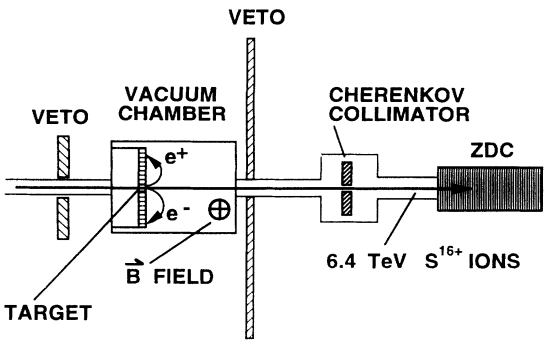

FIG. 1. Schematic of experimental apparatus showing veto detectors, magnetic pair spectrometer, and ion calorimeter detector (ZDC).

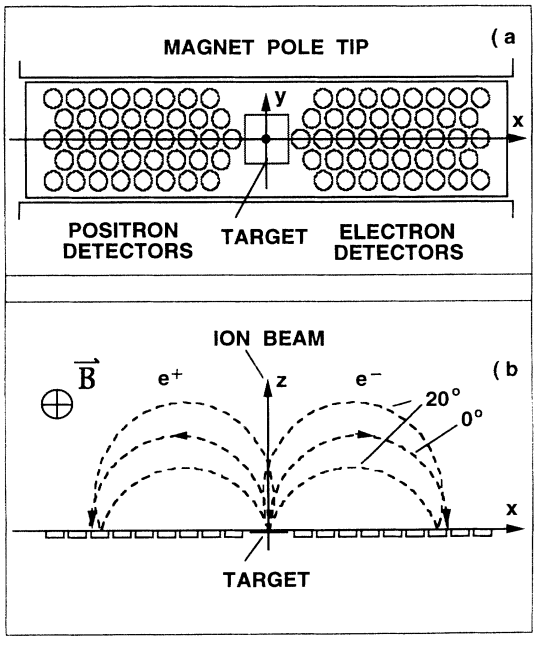

FIG. 2. Schematic of pair spectrometer: (a) End view along beam axis showing target and detector arrays. (b) Top view showing detectors in midplane row and sample trajectories for 5-MeV/c positrons and electrons emitted at 0° and 20° to indicate effects of dispersive plane focusing.

given field setting. The limited vertical height of the array permitted full azimuthal collection only for limited ranges of polar angles which varied from 0°–25° for the innermost (low momentum) detectors to 0°–8° for the outermost (high momentum) detectors. Angular resolution, as determined by finite detector size and vertical spacing, varied from approximately ±8° at low momentum to ±2° at high momentum.

Two large scintillator veto detectors sensitive to minimum ionizing particles, each with a 6-cm-diam central hole, were mounted symmetrically about the beam axis 2 m upstream and downstream of the spectrometer (see Fig. 1). Signals from these detectors were used to veto detector noise counts generated by any high energy particles accompanying the primary ions, but lying in an extended halo >3 cm beyond the main beam axis. A second veto signal was generated for similar halo and scattered high energy particles lying >2 mm and <4 cm from the beam axis, by a quartz Cerenkov active collimator located 5 m downstream, in the WA93 experiment (see Fig. 1).

Electron and positron counts were stored as functions of detector position for two settings of magnetic field (0.18 and 0.45 T) corresponding to detected momenta of 1.0–6.7 and 2.5–17 MeV/c, respectively. Magnetic polarity was also reversed at 0.18 T for comparison of detector response to positrons and electrons. Data were collected for targets of 75-μg/cm^2 polypropylene $(CH_2)_x$; 180-μg/cm^2 Al; 4.9-mg/cm^2 Pd; and 0.6-, 1.5-, and 4.7-mg/cm^2 Au. The very thin targets ($<10^{-3}$ radiation length) were used to minimize backgrounds from direct knock-on (KO) electrons and to avoid significant multiple Coulomb scattering (MCS) of low-energy electrons and positrons.

Less than 1 sulfur ion in 10 000 underwent nuclear-charge-changing collisions in these targets (electromagnetic spallation being the most probable at 2×10^5/ion in the thickest Au target used) [40]. Signals from the WA93 zero-degree calorimeter [41] (ZDC) were used in our experiment to identify, count, and provide timing for full energy projectile sulfur ions. The ZDC separately measured electromagnetic and hadronic stopping components in nine absorption lengths of uranium to obtain an energy resolution of $\sigma/E\approx2\%$, just sufficient to discriminate against ions which have lost one nucleon in close collisions. These signals were employed for normalization and for coincidence measurements with positrons and/or electrons detected in our pair spectrometer.

Signals from each positron and electron detector were amplified by a separate charge-sensitive preamplifier and converted to fast logic pulses (hits) in a timing discriminator. These pulses were counted in coincidence with sulfur ions and in anticoincidence with the various veto signals. Timing between electron and positron signals was also recorded for coincidence event data. Data were taken using a Macintosh II CX controlled acquisition system in which nine parameters per event were stored in list mode for off-line histogram sorting.

Sulfur ions from the SPS were delivered in roughly uniform spills of 5.1 sec length with 10^5 to 10^6 ions per spill. For the 1.5-mg/cm^2 Au target, typical counting rates for 1–7-MeV/c positrons and electrons (primarily KO's) detected in coincidence with projectile ions were (1–10)/sec and (10–1000)/sec, respectively. Variations in data-acquisition efficiencies as functions of counting rates for the various modes of operation were studied by comparing electron and/or positron yields per ion at different ion spill rates and for a number of targets and thicknesses. Positron and electron yields per ion were found to vary linearly with Au target thickness from 0.6 to 4.7 mg/cm^2. No significant nonlinear variations in yields were observed for rates varying over two orders of magnitude.

At small impact parameters (i.e., $\leq\lambda\!\!\!^{-}_c$, the electron Compton wavelength), much heavier ions are expected to produce multiple electron-positron pairs even in single collisions [22,24,25,30]. However, for sulfur ions at 6.4 TeV, production of single pairs is expected to be the only significant mode. The only statistically significant indication of multiple-pair formation observed in the current measurements was identified as arising from electronic pickup of noise signals from other experiment equipment at the SPS accelerator. Such noise-induced bursts generally produced simultaneous signals in most or all of the 82 detector circuits. These multiple-hit background data were rejected by sorting according to a selected detector multiplicity defining a valid event. For data presented here, electron and/or positron detector multiplicities for a valid event were set to unity.

Light targets of polypropylene and aluminum were used to investigate the KO electrons and their effects as backgrounds and to study efficiencies for detection and acquisition under beam-on conditions at electron energies characteristic of both field settings. Efficiencies were determined for each detector in an array by comparison of the measured KO yields with results of Monte Carlo simulations based on relativistic first Born calculations for differential KO cross sections [42]. The average detection efficiency for 1–17-MeV/c electrons found in this way was 46%. We assume here that the efficiency for positron detection by these thin silicon detectors was the same as for electrons of the same energy [41]. Detector efficiencies were also determined during the experiment, at somewhat lower electron energies corresponding to field settings of 0.09 and 0.18 T, through measurements of the β spectrum of a calibrated ^{106}Ru source (end-point energy 3.54 MeV) placed at the target position of the pair spectrometer. Comparison of these results gives an absolute detection efficiency averaged over detectors in an array of (46±9)% for 1–4-MeV/c electrons.

III. RESULTS AND DISCUSSION

A. Singles measurements

We first present results of measurements of electrons and positrons detected independently, but in coincidence with unscattered projectile ions. These "singles" results are used to directly extract singly differential and total cross sections, to quantitatively investigate backgrounds, and to bolster confidence in our interpretations of positron-electron coincidence measurements which will

follow.

As noted previously, the variation in observed counting intensity with vertical (y) displacement is related to the angular distribution of ejected positrons or electrons. The measured distributions represent projections of the source angular differential cross sections on the limited vertical aperture determined by the height of the detector arrays. Electrons and positrons from pairs formed in these peripheral collisions are emitted primarily in the forward direction. Instead of attempting to deconvolute measured distributions, we have mapped selected angular differential cross sections through the magnetic analyzing field to the detector plane and compared the resulting calculated distributions with the data. Using a computer simulation which incorporates effects of multiple Coulomb scattering, and assuming a simple exponential form for the angular cross section [$d\sigma/d\Omega_+ \sim \exp(-\theta/w)$, where θ is the polar angle measured from the beam axis], we have determined $1/e$ angular widths (w) which most closely reproduce the data, as a function of horizontal position (i.e., positron momentum). The exponential form for $d\sigma/d\Omega_+$ was chosen after reviewing several theoretical predictions [21,23] for expected angular distributions. Results of these simulation fits to the data are displayed in Fig. 3 for positrons from a 1.5-mg/cm^2 Au target. All other targets give similar results. Figure 3 also shows results for similar angular widths calculated in an exact Monte Carlo evaluation of the two-photon terms in lowest-order QED calculations for structureless nuclei which are described in Ref. [18], and hereafter referred to as MCQED. Widths from simulation fits to the data differ from the theoretical results by only $\sim 1-2°$, well within the experimental median angular resolution of 3° (excluding MCS angular smearing).

Since the angular distribution for positron emission is peaked so narrowly in the forward direction, the horizontal (x) intensity distribution on the detector array directly represents the momentum distribution. We have summed counts in sets of detectors grouped according to horizontal position and plot overlapping histograms of the resulting momentum distributions in Fig. 4, at the two field settings. The yields have been converted to cross sections and corrected for the fractions of positrons lying outside the vertical acceptance of each detector group. These corrections were made assuming theoretical angular distributions with widths as presented in Fig. 3. Theoretical $d\sigma/dp_+$ cross sections are displayed in Fig. 4 as smooth curves. Results of first Born approximation calculations which employ Sommerfeld-Maue wave functions for the free electron and positron are displayed by the dashed line. To construct this curve, cross sections for 200-GeV protons and uranium targets have been interpolated from Fig. 4 of Ref. 19 and scaled according to Z_P^2 and Z_T^2, where Z_P and Z_T are the projectile and target nucler charges, as directed in Ref. [19]. We note that the first Born results underestimate the cross sections below ~ 3 MeV/c and overestimate them slightly above ~ 8 MeV/c. Results of MCQED calculations are indicated by the solid curve. Agreement is remarkably good up to ~ 4 MeV/c. At higher momenta MCQED gives cross sections as much as 75% higher than the measurements. Linear extrapolation of the first Born cross sections gives a cross section of about 83 b integrated over 1–17 MeV/c. The corresponding MCQED result is 98 b. The measured cross section is 85±22 b, where the error includes statistical and background correction errors and estimated uncertainties in detection and acquisition efficiencies. It does not include any estimate of errors due to uncertainties in corrections made as noted above for incomplete angular acceptance of the pair spectrometer.

Figure 5 shows a comparison of measured momentum-binned yields per sulfur ion for singles elec-

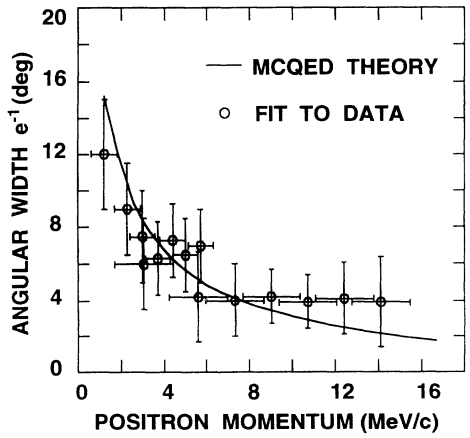

FIG. 3. Angular $1/e$ widths for $d\sigma/d\Omega_+$ plotted as a function of positron momentum for 6.4-TeV S+Au. The data points (○) are results of simulation fits to measured vertical intensity distributions as described in the text. The error bars indicate the observed fitting uncertainty dominated by experimental angular resolution set by detector size. Theoretical results (——) are from MCQED calculations.

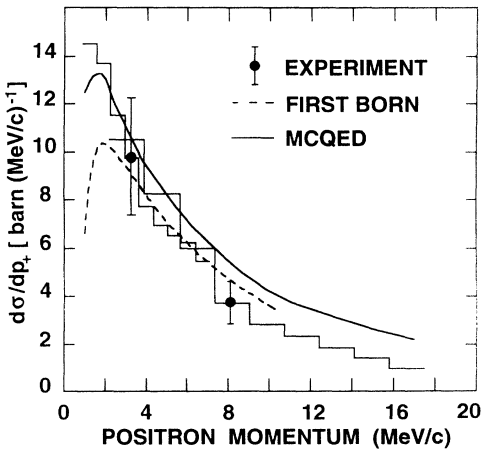

FIG. 4. Measured positron singles cross sections $d\sigma/dp_+$ compared with theoretical results. The overlapping solid line histograms are measured cross sections for field settings of 0.18 and 0.45 T, corrected for incomplete detection of the full angular emission distributions as described in the text. The smooth curves represent results of MCQED calculations (——) and, dashed curve represents interpolations of scaled first Born calculation results (— — —) given in Ref. [23].

trons and positrons from a gold target. No corrections for angular acceptance by the detectors have been made for these data. Assuming pair-produced electrons and positrons have similar momentum distributions, only 2% of the observed singles electrons come from pair production. The other 98% arise from primary KO production and from secondary scattering processes. By using thin, light (polypropylene and aluminum) targets in which pair production is relatively improbable, we have experimentally isolated the KO electron contribution. Yields for KO electrons integrated over all detectors at each field setting vary linearly with electron thickness, given by Z_T number of target atoms/cm^2, independent of Z_T for all targets. We have compared these measured absolute KO yields with results of trajectory calculations based on relativistic Born approximation differential cross sections for binary ion-electron collisions [42]. Our calculations for differential yields agree (within ±25% error) with the light target data, except for the lowest energy (0.6–1.0 MeV) electrons where secondary scattering effects may become important. The calculations also agree well with KO measurements for heavy targets (Pd and Au), especially after correction for the small but significant fraction of electrons from pairs which are primarily emitted in the forward direction. The MCQED calculations predict that ≥80% of pair-produced positrons in the same energy range will intercept the detector array. Calculated KO yields for a 1.5-mg/cm^2 Au target are displayed by the smooth curve in Fig. 5.

Calculations and measurements for KO electrons both exhibit nearly uniform counting distributions along the vertical (y) direction within the detector array. The observed uniformity arises from the narrow angular cuts imposed by the vertical height accepted by the detector array when compared with the relatively larger KO launch angles. Our calculations indicate that only ~20% of all 1–17-MeV/c KO electrons emitted follow paths which intercept the detectors. Most of the low-energy KO's spiral into the aluminum walls of the vacuum chamber downstream of the detectors and lose too much energy in penetrating the metal to continue on trajectories leading back to the detector arrays. Higher energy KO's, which are emitted very forward, proceed further downstream and suffer the same fate. Backgrounds in the positron detectors from scattered KO's are observed to be weak for the low Z_T targets where *real* positron yields are small and KO yields are relatively strong.

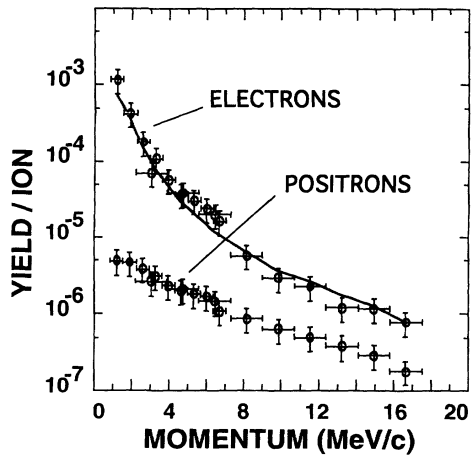

FIG. 5. Measured yields of electrons and positrons from a 1.5-mg/cm^2 Au target detected independently, but in coincidence with 6.4-TeV sulfur ions. The solid curve displays results of Born approximation calculations for binary ion-electron collisons which are described in Ref. [35].

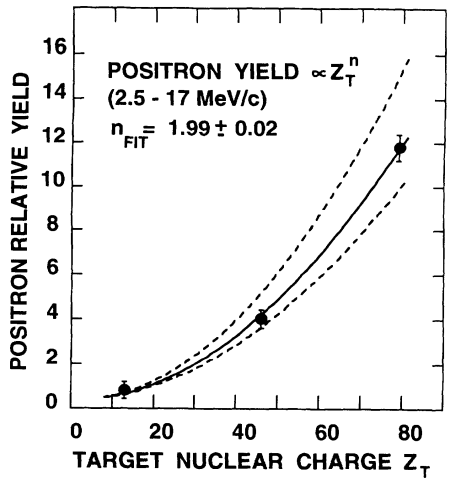

FIG. 6. Measured yields of the positrons per ion per target atom for Al, Pd, and Au, plotted as a function of target nuclear charge. The detected energy range is 2.5–17 MeV. The error bars represent statistical errors and variations in several measurements for a given target element. The power-law fit to the data gives $Z_T^{1.99\pm0.02}$ as depicted by the solid curve. The dashed curves indicate $n = 1.95$ and 2.05.

To examine the dependence of pair production on target nuclear charge Z_T, we have integrated singles positron yields over 2.5–17 MeV/c for targets of Al, Pd, and Au and plotted the resulting relative partial cross sections against Z_T. The results are displayed in Fig. 6. The solid line in the figure represents a least-squares fit proportional to Z_T^n to these data. The fit gives $n = 1.99\pm0.02$. The lower and upper smooth dashed curves represent n values of 1.95 and 2.05, respectively. Cross sections are expected to scale as Z_T^2 by all known first-order theories. Deviation from Z_T^2 scaling might indicate importance of higher-order terms arising from positron-target interaction [31]. Also, significant contributions by KO electron backgrounds would lead to an apparent "positron" yield component linear in Z_T.

B. Electron-positron coincidence measurements

Having established from analysis of the singles data some confidence in our understanding of the angular and momentum distributions for pairs and of KO electrons, the major source of background, we proceed to results deduced from measurements of electrons and positrons detected in time coincidence, i.e., "coincidence" data. Coincidence electron-positron measurements were primarily restricted to gold targets where the pair production-to-KO signal ratios are most favorable. Only very low statistics coincidence data were obtained for the lighter targets and results reported here will concentrate on the gold target measurements. Doubly differential

yields have been obtained by sorting event data into coincidence counts as functions of various parameters calculated from the (41×41) possible pairs of detector positions. To obtain cross sections, corrections have been made for variations in detector efficiencies and for estimated fractions of detector intercepted electrons and positrons, according to assumed extended angular distributions as indicated for singles positrons (see Fig. 3).

As noted for the singles data, the vertical displacement of a detected electron is approximately proportional to the vertical component (p_y) of its transverse momentum. We have sorted event data to determine the relative intensity distributions as a function of pair $(p_{y+}+p_{y-})$ transverse momenta and present the results in Fig. 7. Observed p_y distributions are plotted for both magnetic-field settings representing measured positron (or electron) momenta ranges of 1–7 and 2.5–17 MeV/c, respectively. Both low and high field p_y distributions peak at zero and fall rapidly, with more than 80% of all observed pairs having $p_y \leq 1$ MeV/c. By symmetry, the horizontal component (p_x) of the transverse momentum should have the same intensity distribution. We conclude that pair transverse momenta are small and increase only weakly for higher positron momenta (at least up to ~ 17 MeV/c), and that measured longitudinal (z) momentum distributions therefore well represent the total pair momentum, since the small transverse components approximately cancel.

Figure 8 displays results for $(d^2\sigma/dp_+dp_-)$ for positrons from a gold target in coincidence with the 1–7-MeV/c electrons which were simultaneously detected by the full electron detector array at the low-magnetic-field setting. Comparison with the singles positron cross sections in Fig. 5 shows that the momentum distributions are nearly the same, suggesting, therefore, that positron momenta are almost entirely independent of electron momentum. Tighter cuts on the momenta of coincident electrons yield the same general result. Cross sections $d^2\sigma/dp_+dp_-$ for positrons and for electrons are compared in Fig. 9, where the momentum for the coincident

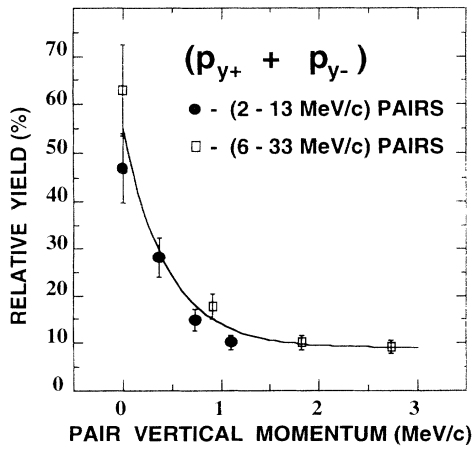

FIG. 7. Transverse vertical momentum $(p_{y+}+p_{y-})$ distributions for detected electron-positron pairs at the two magnetic field settings. The target is gold. The curve is added to guide the eye.

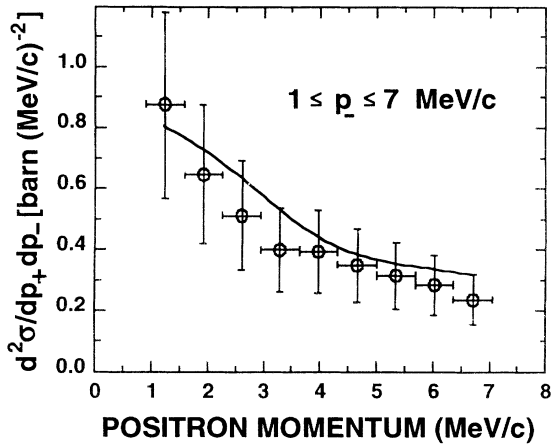

FIG. 8. Doubly differential cross sections $d^2\sigma/dp_+dp_-$ for positrons detected in coincidence with the full momentum range of intercepted electrons at the low-magnetic-field setting. The solid curve shows the relative variation of $d\sigma/dp_+$ taken from the data of Fig. 4. The target is 1.5 mg/cm^2 Au.

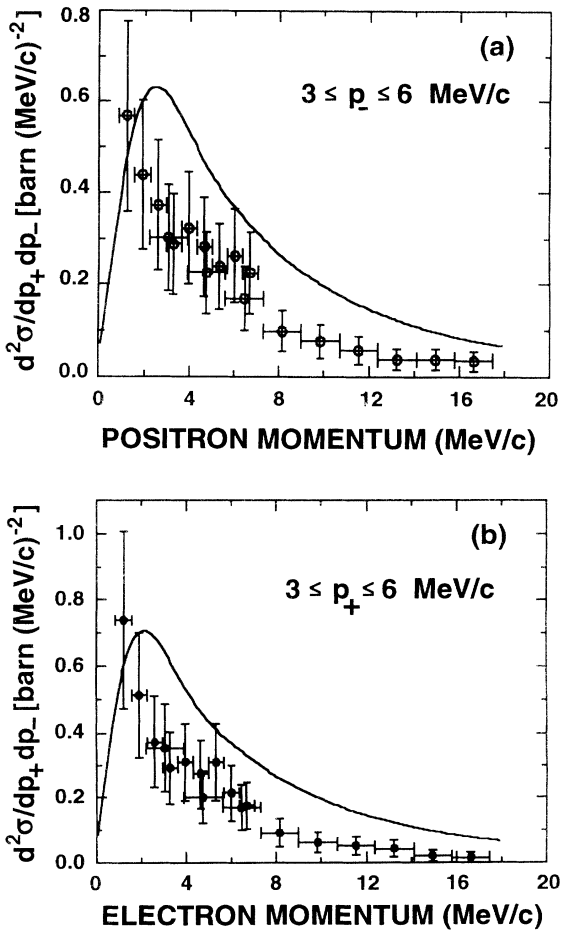

FIG. 9. Doubly differential cross sections $d^2\sigma/dp_+dp_-$ for (a) positrons and for (b) electrons. The momentum range for the coincident pair partner is 3–6 MeV/c in each case. The target is 1.5 mg/cm^2 Au. The curves are first Born results scaled from Ref. [19].

particle has been limited in the sort of the data to 3–6 MeV/c. The smooth curves indicate first-order Born approximation results of Ref. [19], taken from Figs. 1 and 2, interpolated to $\gamma=215$ (200 GeV/nucleon) and scaled as $Z_p^2 Z_T^2$. We note that the calculated cross sections exceed the measured values by as much as $\sim 80\%$, and that measured $d^2\sigma/dp_+ dp_-$ decrease continuously with increasing positron or electron momentum, unlike calculated values which exhibit maxima near 3 MeV/c. The only substantial difference between the measured electron and positron spectra displayed in Fig. 9 is a slight shift in the electron distribution toward low momentum. For momenta ≤ 4 MeV/c, the yield of electrons exceeds that of positrons by 23%. The excess could be explained by coincidences (random and correlated) with low momentum KO electrons, where singles rates (see Fig. 5) are 5 to 100 times larger than for positrons and, hence, for pair-generated electrons. However, the random positron-KO electron coincidence fraction is estimated to be very small for the thin targets used here. A typical randoms-reals fraction calculated from measured singles rates and from the time window defining a coincidence is 10^{-2}, or $\sim 1\%$. Correlated coincidences between positrons and KO electrons could also occur because of secondary KO production by the pair-producing ion, either in ion-electron collisions within the same atom participating in pair production event or in another collision by the same ion in traversing the remaining thickness of the target foil. For typical thickness gold targets, the latter is just the measured (1–17 MeV/c) KO yield per ion which is $\leq 10^{-2}$. We estimate from Born approximation calculations of (primarily K shell) target ionization that the former process will occur $\sim 1\%$ of the time, with less than half of these being detected. Therefore, the sum of random and correlated coincidences between positrons and KO electrons should amount to less than 2% of the real pair coincidences.

Since the KO electrons are expected to account for only a small fraction of the low-energy electron excess observed in the pairs, we have considered alternative explanations. A small horizontal shift ~ 6 mm in the beam position at the target could also lead to the observed asymmetry. However, by reversing the orientation of the magnetic field, we exchanged electron and positron detectors and obtained the same result. Deflections of the ion beam by the analyzing field were insignificant.

The difference between the positron and electron distributions may be attributed instead to a real charge-dependent effect due to the sign difference of the Coulomb potential at the origin of the pair. The $d^2\sigma/dp_+ dp_-$ weighted average kinetic energies taken from the data in Fig. 8 are 4.21 and 3.87 MeV, respectively, for 1–17-MeV/c positrons and electrons. If we interpret in a purely classical picture this (0.34 MeV) shift in the average kinetic energy as arising from a potential-energy difference experienced by the oppositely charged particles at the pair origin, then a rough approximation of the mean distance $\langle b \rangle$ to the gold target nucleus (neglecting screening and the sulfur ion's field) gives $\langle b \rangle \approx 800$ fm or $\sim 2\lambda\!\!\!^{-}_c$, which is consistent with impact parameters expected to be important according to equivalent photon methods [26]. (The 1–17-MeV/c electrons and positrons are localized to $< \lambda\!\!\!^{-}_c$ according to the uncertainty principle.)

We have also investigated the distribution of pair total kinetic energy, by converting the separate momenta of electrons and positrons forming detected pairs to kinetic energies (ε_+ and ε_-). The energies have been combined to give total pair energies $\varepsilon=\varepsilon_+ + \varepsilon_-$, and the corresponding corrected counts have been grouped to give intensity distributions, with the ranges of either component limited by the energies (momenta) covered by all detectors at each field setting. To correct for sorting biases arising from incomplete coverage of all possible momenta (0–17 MeV/c) for the pairs of particles, we have continued our measured data by fitting to a double exponential function as

$$d^2\sigma/dp_+ dp_- \sim e^{-\alpha(p_+ + p_-)} + f e^{-\beta(p_+ + p_-)},$$

where α, β, and f are fitted parameters applicable for all data. The original data plus fitted regions were then sorted with respect to pair kinetic energy ε. Sorts were performed assuming exponential $d^2\sigma/dp_+ dp_-$ extending all the way to zero p_+ and p_- and using a more physically reasonable model in which $d^2\sigma/dp_+ dp_-$ falls smoothly from the measured values obtained at the lowest measured p_+ and p_- to zero at zero p_+ and p_-. Results of the latter method are shown in Fig. 10 for the relative yields of pairs as a function of ε. We note that the yields fall nearly exponentially with no indication of a maximum above 2 MeV, and that 50% of all observed pairs have total kinetic energies below 4 MeV. Theory typically predicts a downturn in the cross section below ~ 4 MeV [44].

These same energy data have been analyzed in the manner described above to determine the fraction of total pair kinetic energy carried away by the positron. Figure 11 shows the probability for energy sharing measured for pairs covered in the two field settings. The error bars represent statistical and efficiency uncertainties for the ratios of binned counts and effects of uncertainties in the fits giving the calculated counts expected in the extended

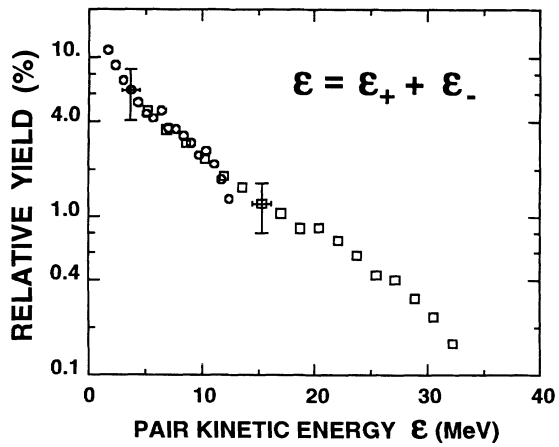

FIG. 10. Relative differential cross section $d\sigma/d\varepsilon$ for pairs of electrons and positrons. ε is the sum of positron and electron kinetic energies.

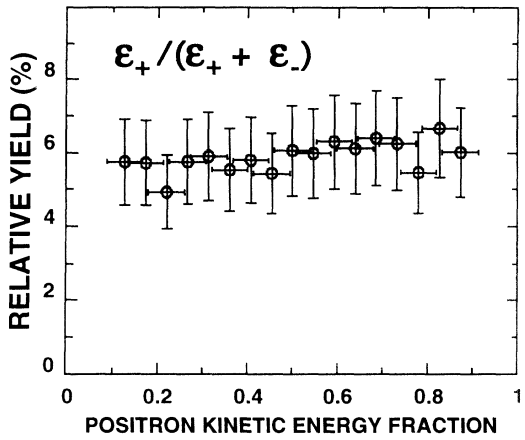

FIG. 11. Probability distribution for energy partitioning between the coincident (1–17 MeV) positrons and electrons forming pairs with energy distribution shown in Fig. 10.

regions of p_+ and p_-. It appears that all modes of partitioning of the energy available are nearly equal probable. Very similar results are obtained in photoproduction [45], the conversion of real γ rays into electron-positron pairs near nuclei. However, there is a weak tendency for positrons to carry slightly more kinetic energy than coincident electrons, consistent with our observations of $p_- = 3$–6 MeV/c.

In summary, the observed projected angular distributions for low-energy positrons are consistent with forward peaked emission with the differential cross section $(d\sigma/d\Omega_+)$ falling to $1/e$ of its peak value for polar angles varying from $\sim 12°$ at 1 MeV/c to $\sim 4°$ at 14 MeV/c. This distribution of angular widths agrees with MCQED calculations for differential cross sections. The positron momentum distribution is peaked below our detection limit of 1 MeV/c and falls to half its observed maximum at ~ 5 MeV/c. First Born calculations tend to underestimate the measured cross section at low momenta, being lower by as much as 35% below 2 MeV/c. MCQED calculations agree well at low momenta, but overestimate the observed cross sections by as much as 80% above 8 MeV/c. Measured cross sections decrease faster at higher momenta than predicted by either calculation. The 1–17-MeV/c positron yield for 6.4-TeV sulfur on gold, corrected for detector efficiencies, integrated over the momentum and angular acceptances set by the detector array dimensions and the magnetic analyzing field, gives an observed cross section of 71 b. Correction for partial angular acceptance versus momentum, based on observed vertical (y) angular distributions within the detection window, raises the measured total cross section to 85 b with an estimated error of $\pm 25\%$. The corresponding MCQED value is 98 b out of a total, integrated over all momenta, of 140 b. Finally, the measured cross sections vary with target nuclear charge as Z_T^2 as predicted by all lowest-order calculations, and relative differential cross sections $d\sigma/dp_+$ are indistinguishable for Al, Pd, and Au targets.

From coincident measurements of positrons and electrons, the pair transverse momentum and total kinetic-energy distributions have been determined. Within limited statistics data for Al and Pd, these distributions are insensitive to target Z_T. Pair transverse momenta are small (< 1 MeV/c) implying that the electron and positron are emitted in the plane of the projectile ion. The pair differential cross-section $d\sigma/d\varepsilon$ falls nearly exponentially from 2–30 MeV, with no indication of a nonzero threshold or maximum above 2 MeV. Momentum distributions for positrons and electrons detected as pairs are similar, with a small relative shift toward lower momenta (kinetic energies) noted for the electrons. Interpreted as a potential difference at the origin, this shift suggests that important impact parameters lie near $\sim 2\lambda\!\!\!^{-}_c$ for production of low-energy pairs. The available excess kinetic energy of the pair is shared between the electron and positron such that all modes are nearly equally populated.

The relatively good agreement between measured $d\sigma/dp_+$ and lowest-order perturbative calculations is expected for 6.4-TeV $S^{16+} + Z_T$ ($Z_T = 13$, 46, and 79), where $Z\alpha \ll 1$, and the probability of producing an electron pair is expected to be small at all impact parameters. It should be noted that this is in contrast to recent results of experiments [37,38] at lower energies for uranium and lanthanum projectiles, where perturbative calculations for electron capture of the pair-produced electrons apparently fail. At higher energies and for the heaviest projectiles, perturbative treatments may also fail, since lower-oder perturbation terms give probabilities for single pair formation which exceed unity at sufficiently small impact parameters. Several theoretical treatments have concluded that multiple pairs will be formed in single close collisions, with some considerable disagreement among the calculations as to the relative strengths of the multiple-pair forming channels [22,24,25,30]. Using perturbation theory values for the probabilities of producing a single pair, several authors [22,25] predict that the number distribution of multiple pairs produced will follow a Poisson distribution. Analysis of nonperturbation expressions for n-pair creation have lead to the same distribution with significant disagreement for absolute cross sections [29]. We will test these predictions in experiments using 33-TeV ($\gamma = 172$) Pb^{82+} ions at the CERN SPS accelerator.

ACKNOWLEDGMENTS

We gratefully acknowledge the invaluable assistance of the CERN SPS staff and of the WA93 collaboration. Without their help and expertise, these measurements would not be possible. We also wish to acknowledge C. Bottcher, M. R. Strayer, and J. C. Wells for MCQED calculations and important discussions regarding interpretation of the data. This research was sponsored by the U.S. Department of Energy, Office of Basic Energy Sciences, Division of Chemical Sciences, under Contract No. DE-AC05-84OR21400 with Martin Marietta Energy Systems, Inc.

[1] H. J. Bhabha, Proc. R. Soc. London, Ser. A **152**, 559 (1935).
[2] G. Racah, Nuovo Cimento **14**, 93 (1937).
[3] L. D. Landau and E. M. Lifshitz, Phys. Z. Sowjetunion **6**, 244 (1934).
[4] T. Murota, A. Ueda, and H. Tanaka, Prog. Theor. Phys. **16**, 482 (1956).
[5] F. F. Ternovskii, Zh. Eksp. Teor. Fiz. **37**, 793 (1960) [Sov. Phys. JETP **10**, 565 (1960)]; **37**, 1010 (1960) [**10**, 718 (1960)].
[6] S. R. Kelner, Yad. Fiz. **5**, 1092 (1966) [Sov. J. Nucl. Phys. **5**, 778 (1967)].
[7] S. R. Kelner and Y. D. Kotov, Yad. Fiz. **7**, 324 (1968) [Sov. J. Nucl. Phys. **7**, 237 (1968)].
[8] A. G. Wright, J. Phys. A **6**, 79 (1973); a critical review of the calculations.
[9] M. M. Block, D. T. King, and W. W. Wada, Phys. Rev. **96**, 1627 (1954).
[10] M. M. Block and D. T. King, Phys. Rev. **95**, 171 (1954).
[11] M. Koshiba and M. F. Kaplan, Phys. Rev. **97**, 193 (1955).
[12] J. E. Naugle and P. S. Freier, Phys. Rev. **104**, 804 (1956).
[13] A. S. Cary, W. H. Barkas, and E. L. Hart, Phys. Rev. D **4**, 27 (1971).
[14] P. L. Jain, M. Kazuno, and B. Girard, Phys. Rev. Lett. **32**, 1460 (1974).
[15] P. L. Jain, M. Kazuno, B. Girard, and Z. Ahmad, Phys. Rev. Lett. **32**, 797 (1974).
[16] J. E. Butt and D. T. King, Phys. Rev. Lett. **31**, 904 (1973).
[17] L. R. Fortney, A. T. Goshaw, J. W. Lamsa, J. S. Loos, D. A. Niemi, W. J. Robertson, and W. D. Walker, Phys. Rev. Lett. **34**, 907 (1975).
[18] J. D. Jackson, *Classical Electrodynamics* (Wiley, New York, 1962), Chap. 15.
[19] K. F. Weizsäcker, Z. Phys. **88**, 612 (1934).
[20] E. J. Williams, Phys. Rev. **45**, 729 (1934).
[21] C. Bottcher and M. R. Strayer, Phys. Rev. D **39**, 1330 (1989).
[22] M. J. Rhoades-Brown and J. Weneser, Phys. Rev. A **44**, 330 (1991).
[23] F. Decker, Phys. Rev. A **44**, 2883 (1991); F. Decker and J. Eichler, *ibid.* **45**, 3343 (1992).
[24] K. Rumrich, K. Momberger, G. Soff, W. Greiner, N. Grün, and W. Scheid, Phys. Rev. Lett. **66**, 2613 (1991).
[25] G. Baur and C. A. Bertulani, Phys. Rev. C **35**, 836 (1987); G. Baur, Phys. Rev. A **42**, 5736 (1990).
[26] J. Eichler, Phys. Rep. **193**, 167 (1990); a review of theoretical progress to 1990.
[27] P. B. Eby, Phys. Rev. A **43**, 2258 (1991); **39**, 2374 (1989).
[28] K. Kajantie, M. Kataja, L. McLevran, and P. V. Ruuskanen, Phys. Rev. D **34**, 811 (1986); K. Kajantie, J. Kapusta, L. McLevran, and A. Mekjian, *ibid.* **34**, 2746 (1986).
[29] C. Best, W. Greiner, and G. Soff, Phys. Rev. A **46**, 261 (1992).
[30] J. C. Wells, V. E. Oberacker, A. S. Umar, C. Bottcher, M. R. Strayer, J.-S. Wu, and G. Plunien, Phys. Rev. A **45**, 6296 (1992).
[31] D. C. Ionescu and J. Eichler, Phys. Rev. A **48**, 1176 (1993).
[32] H. Gould, in *Atomic Theory Workshop on Relativistic and QED Effects in Heavy Atoms,* edited by Hugh P. Kelly and Yong-ki Kim, AIP Conf. Proc. No. 136 (AIP, New York, 1985).
[33] C. Bottcher and M. R. Strayer, in *Physics of Strong Fields,* Vol. 153, of *NATO Advanced Study Institute, Series B: Physics,* edited by W. Greiner (Plenum, New York, 1987), p. 629.
[34] E. Teller, Nucl. Instrum. Meth. Phys. Res. B **24/25**, 3 (1987).
[35] C. R. Vane, S. Datz, P. F. Dittner, H. F. Krause, C. Bottcher, M. Strayer, R. Schuch, H. Gao, and R. Hutton, Phys. Rev. Lett. **69**, 1911 (1992).
[36] J. H. Derrickson *et al.*, in *Proceedings of the Twenty-First International Cosmic Ray Conference* (R. J. Prothero, University of Adelaide, Adelaide, Australia, 1990).
[37] A. Belkacem, H. Gould, B. Feinberg, R. Bossingham, and W. E. Meyerhof, Phys. Rev. Lett. **71**, 1514 (1993).
[38] A. Belkacem, H. Gould, B. Feinberg, R. Bossingham, and W. E. Meyerhof, *The Physics of Electronic and Atomic Collisions,* edited by T. Andersen, B. Fastrup, F. Folkmann, H. Knudsen, and N. Andersen (AIP, New York, 1993).
[39] H Gutbrod *et al.*, CERN Report No. SPSLC 91-17 SPSLC/P/260, 1991 (unpublished).
[40] B. Price, Ren Guoxiao, and W. T. Williams, Phys. Rev. Lett. **61**, 2193 (1988).
[41] G. R. Young *et al.*, Nucl. Instrum. Methods A **279**, 503 (1989).
[42] C. R. Vane, S. Datz, P. F. Dittner, H. F. Krause, C. Bottcher, M. Strayer, R. Schuch, H. Gao, and R. Hutton, Nucl. Instrum. Methods Phys. Res. B **79**, 26 (1993).
[43] Th. Frommhold *et al.*, Nucl. Instrum. Methods A **310**, 657 (1991).
[44] For example, see Fig. 6 of Ref. [27].
[45] W. Heitler, *The Quantum Theory of Radiation,* 3rd. ed. (Oxford University, London, 1954); C. F. Powell, P. H. Fowler, and D. H. Perkins, *The Study of Elementary Particles by the Photographic Method* (Pergamon, New York, 1959), p. 181.